Spin distribution of nuclear levels using the static path approximation with the random-phase approximation

K. Kaneko[1,*] and A. Schiller[2]

[1]*Department of Physics, Kyushu Sangyo University, Fukuoka 813-8503, Japan*

[2]*National Superconducting Cyclotron Laboratory, Michigan State University, East Lansing, Michigan 48824, USA*

(Received 12 December 2006; published 12 April 2007)

We present a thermal and quantum-mechanical treatment of nuclear rotation using the formalism of the static path approximation plus the random-phase approximation. Naive perturbation theory fails because of the presence of zero-frequency modes resulting from dynamical symmetry breaking. Such modes lead to infrared divergences. We show that composite zero-frequency excitations are properly treated within the collective coordinate method. The resulting perturbation theory is free from infrared divergences. Without the assumption of individual random spin vectors, we derive microscopically the spin distribution of the level density. The moment of inertia is thereby related to the spin-cutoff parameter in the usual way. Explicit calculations are performed for ^{56}Fe; various thermal properties are discussed. In particular, we demonstrate that the increase of the moment of inertia with increasing temperature is correlated with the suppression of pairing correlations.

DOI: 10.1103/PhysRevC.75.044304 PACS number(s): 21.60.Jz, 21.10.Ma, 05.30.−d

I. INTRODUCTION

The spin distribution of nuclear levels is important for Hauser-Feshbach-type calculations of astrophysical reaction rates [1]. Generally, the spin distribution of nuclear levels is assumed to be given by

$$\rho(E, I) = \rho(E)\frac{2I+1}{2\sigma^2}e^{-\frac{I(I+1)}{2\sigma^2}} \quad (1)$$

$$= W(E)\frac{2I+1}{2\sqrt{2\pi}\sigma^3}e^{-\frac{I(I+1)}{2\sigma^2}}, \quad (2)$$

where $\rho(E, I)$ is the level density for a given spin I and σ is the spin-cutoff parameter [2–6]. It should be noted that the total level density (summed over all spins) is given by $\rho(E) = \Sigma_I \rho(E, I)$, whereas the total state density given by $W(E) = \Sigma_I(2I+1)\rho(E, I)$ contains an additional factor $2I+1$ for each level to take into account the m degeneracy. In deriving the spin distribution, one typically assumes that the individual nucleon spins are pointing in random directions; hence the spin distribution becomes Gaussian and can be described by only one parameter, the spin-cutoff parameter. This parameter can be related to the moment of inertia $\mathcal{J}_{\text{rigid}}$ by

$$\sigma^2 = \frac{\mathcal{J}_{\text{rigid}}T}{\hbar^2}, \quad (3)$$

where T is the thermodynamical temperature [7]. This result can be derived within an independent-particle model with individual nucleon spins but with correlations neglected [7]. Microscopic calculations of the spin distribution are difficult to perform when correlations are present. Experimental data on the spin-cutoff parameter are available only in a few cases [4]. Therefore, theoretical predictions of the spin-cutoff parameter are greatly desired. Alhassid *et al*. have recently investigated the spin distribution in the framework of the shell-model Monte Carlo (SMMC) [8,9] and the static path approximation (SPA) methods [8]. Assuming that the spin distribution can be described by Eq. (2), they found a significant suppression of the moment of inertia and an odd-even staggering of the spin-cutoff parameter from pairing correlations at low excitation energies.

The SPA method [8,10–12] is a useful treatment to evaluate approximately the partition function of finite systems with separable interactions such as the pairing plus quadrupole-quadrupole (P+QQ) interaction, and it provides exact result at high temperatures. However, as temperatures decrease the SPA becomes inaccurate because quantal fluctuations around the mean field can no longer be neglected. In leading order perturbation theory, small-amplitude fluctuations give corrections to the partition function that can be treated by random-phase approximation (RPA) [13–16].

However, such a perturbative treatment exhibits an infrared problem in the case where the nucleus is modeled in terms of independent nucleons moving in a deformed mean field: There are zero-frequency modes among normal vibrational modes. This can be understood because the SPA method breaks the symmetry of rotational invariance for a deformed nucleus. It operates in a body-fixed reference frame that undergoes time-dependent transformations. The collective (zero-frequency) excitation (i.e., the motion of the rotating frame) is treated on an equal footing with other excitations. This leads to a Lagrangian that displays local symmetry, yielding the mechanical equivalent of gauge invariance. The collective coordinate method developed by Gervais and Sakita [17] treats the inherent symmetries of the problem consistently. It separates the so-called spurious motions from the intrinsic vibrations. In the laboratory frame, these zero-frequency excitations are not really spurious; they represent a rotational motion that has to be treated separately.

In the present paper, we describe microscopically the nuclear rotation of a deformed nucleus including thermal and quantal fluctuations using the SPA+RPA method, and we derive the associated spin distribution of nuclear levels. First, by using the collective coordinate method, the rotation

*Electronic address: kaneko@ip.kyusan_u.ac.jp

is described in terms of the zero-frequency modes that emerge from the breaking of rotational invariance of the deformed mean field. Second, the spin distribution of nuclear levels is calculated by a proper treatment of the zero-frequency modes in the framework of the SPA+RPA method. In Sec. II, the collective coordinate method is applied to the partition function of an interacting fermion system. In Sec. III we show how to calculate the partition function of the P+QQ model using the SPA+RPA method. In Sec. IV, we present a correct treatment of the zero-frequency modes and derive the spin-dependent level density. In Sec. V, the model is applied to ^{56}Fe and related thermal properties are investigated. Concluding remarks are given in Sec. VI.

II. THE COLLECTIVE COORDINATE METHOD

According to the theory developed by Gervais, Jevicki, and Sakita [18], a problem involving only fermion degrees of freedom can be transformed into an equivalent, constraint problem including both fermion and collective degrees of freedom. Concerning the problem at hand, a perturbative treatment of nuclear rotation within the path integral formalism has been proposed by using the collective coordinate method [19,20]. Let us consider a partition function of an interacting fermion system given by the path integral after Wick rotation,

$$Z = \int \prod_{\alpha} \mathcal{D}[c_\alpha^\dagger]\mathcal{D}[c_\alpha] e^{-S_E(\beta)}. \tag{4}$$

Here, the action $S_E(\beta)$ is given by

$$S_E(\beta) = \int_0^\beta \left(\sum_\alpha c_\alpha^\dagger \dot{c}_\alpha + H(c^\dagger, c) \right) d\tau, \tag{5}$$

where $\beta = 1/T$ is the inverse temperature and the dot indicates a derivative with respect to the imaginary time τ. The antiperiodic boundary condition $c(\beta) = -c(0)$ arises since the fermionic nature of the field means the operators c are Grassmann numbers. The action $S_E(\beta)$ is rotationally invariant with respect to the SO(3) algebra.

We shall now be concerned with the case in which the fermion system becomes deformed and breaks the SO(3) invariance. As mentioned in Sec. I, a naive perturbative treatment fails because of the presence of zero-frequency modes. A better way to tackle this problem is to introduce collective coordinates. We therefore adopt the path integral formulation of Gervais and Sakita [17]. To separate the collective coordinates, we employ the equality

$$\begin{aligned} 1 = & \int \prod_i \mathcal{D}[L_i]\mathcal{D}[\phi_i]\delta(\hbar L_i - J_i(b^\dagger, b)) \\ & \times \delta(\Theta_i(b^\dagger, b))\det[J, \Theta]_{\mathrm{PB}}, \end{aligned} \tag{6}$$

where $\Theta_i(b^\dagger, b)$ is an arbitrary function of the fermion fields $(b^\dagger, b)$ with the condition that the determinant of the Poisson bracket $[\,]_{\mathrm{PB}}$ does not vanish. The fermion fields in the body-fixed frame $(b^\dagger, b)$ are obtained by a linear transformation from the laboratory frame,

$$b_\alpha(\phi_i) = P_{\mathrm{R}}(\phi_i) c_\alpha P_{\mathrm{R}}(\phi_i)^{-1}, \tag{7}$$

where $P_{\mathrm{R}}(\phi_i)$ is the rotational operator with the Euler angles $\phi_i (i = 1, 2, 3)$, and L_i are the three components of the collective angular momentum.

Inserting Eq. (6) into the right-hand side of Eq. (4) and exploiting the constraint $\hbar L_i = J_i(b^\dagger, b)$, one finds

$$\begin{aligned} Z = & \int \prod_\alpha \mathcal{D}[b_\alpha^\dagger]\mathcal{D}[b_\alpha] \int \prod_i \mathcal{D}[L_i]\mathcal{D}[\phi_i] \\ & \times \exp\left(-S_E(\beta) + \int_0^\beta \sum_j \prod_j (\tau)\dot{\phi}_j(\tau) d\tau \right) \\ & \times \delta(\hbar L_i - J_i(b^\dagger, b))\delta(\Theta_i(b^\dagger, b))\det(V)\det[J, \Theta]_{\mathrm{PB}}, \end{aligned} \tag{8}$$

where Π_i are conjugates of the angular variables ϕ_i defined by the linear transformation

$$\prod_i = \sum_j V_{ij} L_j, \tag{9}$$

$$V = \begin{pmatrix} -\sin\phi_2 \cos\phi_3 & \sin\phi_3 & 0 \\ \sin\phi_2 \sin\phi_3 & \cos\phi_3 & 0 \\ \cos\phi_2 & 0 & 1 \end{pmatrix}. \tag{10}$$

Let us now define Z_I by imposing on Eq. (8) the boundary condition $L_i \to I_i$ for $\tau \to 0$ or β, where the total angular momentum I is given by $I = \sqrt{\Sigma_i I_i^2}$. Then the path integral over ϕ_i and L_i can be computed by standard methods:

$$\begin{aligned} Z_I = & \int d^3 I \int \prod_\alpha \mathcal{D}[b_\alpha^\dagger]\mathcal{D}[b_\alpha] e^{-S_E(\beta)} \delta\left(I - \sqrt{\sum_i I_i^2} \right) \\ & \times \delta(\hbar I_i - J_i(b^\dagger, b))\delta(\Theta_i(b^\dagger, b))\det[J, \Theta]_{\mathrm{PB}}. \end{aligned} \tag{11}$$

It is now useful to specify the $\Theta_i(b^\dagger, b)$ as the conjugate angular variables of the $J_i(b^\dagger, b)$. Then, the gauge condition $\delta(\Theta_i(b^\dagger, b))$ fixes the position of the intrinsic frame of reference relative to the rotating body. This eliminates rotations of the system as degrees of freedom associated with the fermion fields. However, the components I_i of angular momentum in the intrinsic frame depend upon the choice of the gauge angular variables $\Theta_i(b^\dagger, b)$.

III. MODEL

A. The P+QQ Hamiltonian

Let us consider the P+QQ Hamiltonian [21,22] as a model Hamiltonian

$$H = H_{\mathrm{s.p.}} - GP^\dagger P - \frac{\chi}{2} \sum_\mu Q_{2\mu}^\dagger Q_{2\mu}, \tag{12}$$

$$H_{\mathrm{s.p.}} = \sum_\alpha \varepsilon_\alpha c_\alpha^\dagger c_\alpha, \tag{13}$$

$$P = \sum_{\alpha} c_{\bar{\alpha}} c_{\alpha}, \tag{14}$$

$$Q_{2\mu} = \sum_{\alpha} \langle \alpha | r^2 Y_{2\mu} | \beta \rangle c^{\dagger}_{\alpha} c_{\beta}, \tag{15}$$

where $H_{\text{s.p.}}$ is a single-particle Hamiltonian, P is the monopole pairing operator, G is the strength of the pairing interaction, $Q_{2\mu}$ are components of the mass quadrupole tensor, and χ is the strength of the quadrupole-quadrupole interaction. This model has been applied to the SPA+RPA method including thermal and quantal fluctuations [23].

B. The Hubbard-Stratonovich transformation

By using the Hubbard-Stratonovich transformation [24]

$$\begin{aligned} \text{const} &= \int \mathcal{D}\zeta^* \mathcal{D}\zeta \prod_{\mu} \mathcal{D}[\sigma^*_{\mu}] \mathcal{D}[\sigma_{\mu}] \\ &\quad \times \exp\left[\int_0^{\beta} d\tau G(\zeta^* - P^{\dagger})(\zeta - P) \right] \\ &\quad \times \exp\left[\int_0^{\beta} d\tau \frac{\chi}{2} \sum_{\mu} (\sigma^*_{\mu} - Q^{\dagger}_{2\mu})(\sigma_{\mu} - Q_{2\mu}) \right], \end{aligned} \tag{16}$$

the partition function of Eq. (11) can be written as the auxiliary field path integral [15,25]

$$\begin{aligned} Z_I &= \int d^3 I \int \mathcal{D}\zeta^* \mathcal{D}\zeta \int \prod_{\mu} \mathcal{D}[\sigma^*_{\mu}] \mathcal{D}[\sigma_{\mu}] \text{Tr}[e^{-\beta H'}] \\ &\quad \times \exp\left[\int_0^{\beta} d\tau \left(-\frac{|\zeta|^2}{G} - \frac{\chi}{2} |\sigma_{\mu}|^2 \right) \right] \\ &\quad \times \delta\left(I - \sqrt{\sum_i I_i^2} \right) \\ &\quad \times \delta(\hbar I_i - J_i(b^{\dagger}, b)) \delta(\Theta_i(b^{\dagger}, b)) \det[J, \Theta]_{\text{PB}}, \end{aligned} \tag{17}$$

where

$$\text{Tr}[e^{-\beta H'}] = \int \prod_{\alpha} \mathcal{D}[b^{\dagger}_{\alpha}] \mathcal{D}[b_{\alpha}] \exp\left[-\int_0^{\beta} d\tau H' \right], \tag{18}$$

$$H' = H_{\text{s.p.}} - \zeta P^{\dagger} - \zeta^* P - \chi \sum_{\mu} \sigma_{\mu} Q^{\dagger}_{2\mu}. \tag{19}$$

C. The SPA+RPA method

In the perturbative expansion of the partition function Z_I around the static fields, the zeroth-order term gives the Hartree-like solution, whereas the second-order terms lead to the RPA corrections. This approximation may be largely improved by applying it to all time-independent paths of ζ and σ_{μ}. We therefore expand the partition function (17) around the static paths $\bar{\zeta}$ and $\bar{\sigma}_{\mu}$ in Fourier series,

$$\zeta = \bar{\zeta} + \sum_{n \neq 0} \xi_n e^{-i\omega_n \tau}, \tag{20}$$

$$\sigma_{\mu} = \bar{\sigma}_{\mu} + \sum_{n \neq 0} \eta_{\mu n} e^{-i\omega_n \tau}, \tag{21}$$

where $\omega_n = 2\pi n/\beta$ are the Matsubara frequencies. Let us now define the principal axis of the quadrupole potential in the intrinsic frame by $\bar{\sigma}_0 = \hbar\omega_0 \beta_2 \cos\gamma$, $\bar{\sigma}_2 = \bar{\sigma}_{-2} = \hbar\omega_0 \beta_2 \sin\gamma/\sqrt{2}$, and $\bar{\sigma}_1 = \bar{\sigma}_{-1} = 0$, where $\hbar\omega_0 = 41\text{MeV}/A^{1/3}$. The pairing fields can be rewritten as $\bar{\zeta} = \Delta e^{-\psi}$ by using real values Δ and ψ.

It is now convenient to introduce quasiparticles by diagonalizing the Hamiltonian of Eq. (19):

$$\begin{pmatrix} a \\ a^{\dagger} \end{pmatrix} = \mathcal{W}^{\dagger} \begin{pmatrix} b \\ b^{\dagger} \end{pmatrix} = \begin{pmatrix} \bar{U}^{\dagger} & \bar{V}^{\dagger} \\ \bar{V}^{T} & \bar{U}^{T} \end{pmatrix} \begin{pmatrix} b \\ b^{\dagger} \end{pmatrix}, \tag{22}$$

where the matrix $\mathcal{W}$ satisfies the unitarity condition $\mathcal{W}^{\dagger}\mathcal{W} = 1$. According to the Bloch-Messiah theorem [26], this unitary matrix can be decomposed into three matrices:

$$\mathcal{W} = \begin{pmatrix} D & 0 \\ 0 & D^* \end{pmatrix} \begin{pmatrix} U & V \\ V & U \end{pmatrix} \begin{pmatrix} C & 0 \\ 0 & C^* \end{pmatrix}. \tag{23}$$

The first transformation D is determined by diagonalizing the deformed term of Eq. (19):

$$\begin{aligned} H_{\text{def}} &= H_{\text{s.p.}} - \chi \sum_{\mu} \bar{\sigma}_{\mu} Q^{\dagger}_{2\mu} \\ &= H_{\text{s.p.}} - \hbar\omega_0 \beta_2 \\ &\quad \times \left(Q_{20} \cos\gamma + \frac{Q_{22} + Q_{2-2}}{\sqrt{2}} \sin\gamma \right), \end{aligned} \tag{24}$$

from which we obtain the deformed fermion fields

$$d_k = \sum_{\alpha} D_{k,\alpha} b_{\alpha}, \tag{25}$$

where $D_{k,\alpha}$ are the matrix elements obtained by solving the eigenvalue problem $H_{\text{def}}|k\rangle = \varepsilon_k |k\rangle$. Now, the Hamiltonian H' of Eq. (19) can be simplified to

$$H' = \sum_{k} \varepsilon_k d^{\dagger}_k d_k - \Delta(P^{\dagger} + P). \tag{26}$$

The matrices U and V of Eq. (23) diagonalize the pairing term of Eq. (26). The matrices are diagonal and determined by solving the Hartree-Fock-Bogolyubov equations

$$\begin{pmatrix} \bar{\varepsilon}_k & \Delta \\ \Delta & -\bar{\varepsilon}_k \end{pmatrix} \begin{pmatrix} u_k \\ v_k \end{pmatrix} = E_k \begin{pmatrix} u_k \\ v_k \end{pmatrix}, \tag{27}$$

where E_k are the quasiparticle energies.

In a small system such as the nucleus in which the particle number is strictly fixed, the canonical partition function should be employed. However, exact number projection is difficult to implement in the SPA+RPA formalism; it is easier to apply number-parity projection. Performing the Gaussian integral over ξ_n and $\eta_{\mu n}$ in second-order perturbation theory and introducing the number-parity projection $P_s = (1 + s e^{i\pi N})/2$,

where s denotes the even or odd number parity [15], we obtain the partition function

$$Z_{s,I} = \frac{2\beta}{G}\left(\frac{\kappa\beta}{2\pi}\right)^{5/2}\int_0^\infty d\Delta\Delta \times \int_0^\infty d\beta_2\beta_2^4\int_0^{\pi/3} d\gamma|\sin(3\gamma)| \times 4\pi I^2 \exp\left[-\left(\frac{\Delta^2}{G}+\frac{1}{2}\kappa\beta_2^2\right)\beta\right]\mathrm{Tr}[P_s e^{-\beta H'}] \times \delta(\hbar I_i - J_i(a^\dagger,a))\delta(\Theta_i(a^\dagger,a))\det[J,\Theta]_{\mathrm{PB}} C_{\mathrm{RPA}}, \quad (28)$$

where the parameter $\kappa = (\hbar\omega_0/b^2)^2/\chi$ and $b \propto A^{1/3}$ is the harmonic oscillator length. The expression (28) contains both the static mean-field contributions and the associated Gaussian corrections. These small-amplitude quantal corrections are included in the factor

$$C_{\mathrm{RPA}} = C_{\mathrm{RPA}}(Q)C_{\mathrm{RPA}}(\Delta), \quad (29)$$

where $C_{\mathrm{RPA}}(Q)$ and $C_{\mathrm{RPA}}(\Delta)$ are the corrections from the QQ and pairing correlations, respectively. The SPA partition function is obtained by neglecting these RPA corrections. $C_{\mathrm{RPA}}(Q)$ is explicitly given by

$$C_{\mathrm{RPA}}(Q) = \prod_{n>0}\det(1-\chi R(\omega_n))^{-1}. \quad (30)$$

Here $R(\omega_n)$ is the response function matrix given by

$$R(\omega_n) = \sum_{kl}\frac{Q_{kl}Q_{kl}(E_k+E_l)(1-f_k-f_l)}{(E_k+E_l)^2+\omega_n^2} + \sum_{kl}\frac{\tilde{Q}_{kl}\tilde{Q}_{kl}(E_k-E_l)(f_k-f_l)}{(E_k-E_l)^2+\omega_n^2}, \quad (31)$$

$$Q_{kl} = q_{kl}(u_k v_l + v_k u_l), \quad (32)$$

$$\tilde{Q}_{kl} = q_{kl}(u_k u_l - v_k v_l), \quad (33)$$

where q_{kl} are quadrupole matrix elements and f_k are Fermi occupation probabilities [$f_k = (1+e^{\beta E_k})^{-1}$]. The response function can be calculated by solving the dispersion equation $\det(1-\chi R(i\omega_n)) = 0$. It can be also obtained by diagonalizing the finite-temperature RPA equations [27,28]

$$\langle[H_{\mathrm{RPA}}(Q), O_\nu^\dagger]\rangle = \hbar\Omega_\nu\langle O_\nu^\dagger\rangle, \quad (34)$$

where Ω_ν are the RPA frequencies and the RPA modes are defined by

$$O_\nu^\dagger = \sum_{kl}\left(X_{kl}^\nu a_k^\dagger a_l^\dagger - Y_{kl}^\nu a_l a_k\right) + \sum_{kl}\left(Z_{kl}^\nu a_k^\dagger a_l - \bar{Z}_{kl}^\nu a_l^\dagger a_k\right). \quad (35)$$

The symbol $\langle\,\rangle$ in Eq. (34) denotes thermal averaging with respect to quasiparticles according to Wick's theorem

$$\langle F\rangle = \mathrm{Tr}\left[F\exp\left(-\beta\sum_k E_k a_k^\dagger a_k\right)\right]\Big/ Z_{\mathrm{qp}}, \quad (36)$$

$$Z_{\mathrm{qp}} = \mathrm{Tr}\left[\exp\left(-\beta\sum_k E_k a_k^\dagger a_k\right)\right], \quad (37)$$

where, as an an example, we give $\langle a_k^\dagger a_l\rangle = \delta_{kl} f_k$. At this point, it would be more correct to use thermal average and Fermi occupation probabilities in number-parity projection instead, but the corresponding corrections in the RPA are normally small and would not change our conclusions. It would be important for the odd-even effects in the moment of inertia [8]. The RPA Hamiltonian $H_{\mathrm{RPA}}(Q)$ can now be expressed in the diagonal form

$$H_{\mathrm{RPA}}(Q) = \sum_\nu \hbar\Omega_\nu O_\nu^\dagger O_\nu. \quad (38)$$

There are, however, zero-frequency modes $O_{\nu=0}$ owing to the symmetry breaking of the deformed Hartree solutions on the static path. The correct treatment of these modes will be given in the next section. The RPA correction $C_{\mathrm{RPA}}(Q)$ can now be written exactly in terms of the RPA frequencies Ω_ν as

$$C_{\mathrm{RPA}}(Q) = \frac{\prod'_{kl}\frac{1}{(E_k+E_l)}\sinh\frac{\beta(E_k+E_l)}{2}}{\prod_\nu\frac{1}{\Omega_\nu}\sinh\frac{\beta\Omega_\nu}{2}}, \quad (39)$$

where the prime in Π'_{kl} denotes the restriction of the product to pairs (k,l) that satisfy the conditions $k<l$ and $E_k+E_l \neq 0$. Note that for deformed or heavy nuclei there are many RPA frequencies Ω_ν in the numerator and many E_k+E_l pairs in the denominator.

The pairing RPA correction $C_{\mathrm{RPA}}(\Delta)$ is obtained in a similar way as $C_{\mathrm{RPA}}(Q)$ by

$$C_{\mathrm{RPA}}(\Delta) = \prod_k \frac{\omega_k\sinh[\beta E_k]}{2E_k\sinh[\beta\omega_k/2]}. \quad (40)$$

Here, ω_k are the conventional thermal RPA energies and $E_k = \sqrt{\varepsilon_k'^2+\Delta^2}$ with $\varepsilon_k' = \varepsilon_k - \mu - G/2$.

IV. ROTATIONAL MOTION AND ZERO-FREQUENCY MODES

We consider the two-body Hamiltonian H that is invariant under a continuous rotational operation generated by the angular momentum operators J_i. However, the deformed solutions on the static path violate this symmetry and lead to zero-frequency modes that are regarded as spurious modes in the intrinsic frame. Then, the rotational invariance must be restored by the residual interaction, which is defined as the difference between the exact and the mean-field Hamiltonian. Proper inclusion of the residual interaction will therefore restore the rotational invariance and will provide the rotational energy. To achieve this goal, we present in this section the correct treatment of zero-frequency modes within the

finite-temperature RPA. It is shown that the zero-frequency modes in the intrinsic frame are not spurious in the laboratory frame and correspond to three-dimensional rotational motions.

A. Treatment of zero-frequency modes

For the calculation of the partition function of the constraint system [see Eq. (28)], we follow the treatment proposed by Marshalek and Weneser [29]. For the sake of simplicity, we assume an axially symmetric mean field for the deformed Hartree calculation with one violated symmetry and neglect the γ degree of freedom. In particular, we consider the case where the symmetry is violated for rotations around the x axis, which is perpendicular to the symmetry or z axis. Three-dimensional rotation can be treated in a similar way.

When the eigenvalue equation (34) has zero-frequency solutions because of the breaking of rotational invariance in the intrinsic frame,[1] the usual treatment is known to cause problems concerning the completeness and normalization. Therefore, instead of O_ν and $O_\nu^\dagger$, we define the following coordinate and conjugate momenta:

$$p_\nu = \sqrt{\frac{\hbar\Omega_\nu}{2}}(O_\nu + O_\nu^\dagger), \tag{41}$$

$$q_\nu = i\sqrt{\frac{\hbar}{2\Omega_\nu}}(O_\nu - O_\nu^\dagger). \tag{42}$$

The finite-temperature RPA equations are then expressed as

$$\langle[H_{\mathrm{RPA}}, q_\nu]_{\mathrm{PB}}\rangle = -i\hbar\langle p_\nu\rangle, \tag{43}$$

$$\langle[H_{\mathrm{RPA}}, p_\nu]_{\mathrm{PB}}\rangle = i\hbar\Omega_\nu^2\langle q_\nu\rangle. \tag{44}$$

For the zero-frequency mode $O_{\nu=0}$ in the finite-temperature RPA equations (34), the angular momentum J_x and the canonical conjugate angle coordinate Θ_x are defined by $J_x = \mathcal{J}_x^{1/2} p_0$ and $\Theta_x = \mathcal{J}_x^{-1/2} q_0$, respectively, where $\mathcal{J}_x$ is the moment of inertia. Θ_x and $\mathcal{J}_x$ can be determined by solving the equations of motion

$$\langle[H_{\mathrm{RPA}}, \Theta_x]_{\mathrm{PB}}\rangle = \frac{-i\hbar}{\mathcal{J}_x}\langle J_x\rangle, \tag{45}$$

$$\langle[\Theta_x, J_x]_{\mathrm{PB}}\rangle = i\hbar, \tag{46}$$

where Eq. (45) simply corresponds to the self-consistency condition $\dot{\Theta}_x = [H_{\mathrm{RPA}} - J_x^2/2\mathcal{J}_x, \Theta_x]_{\mathrm{PB}} = 0$, and we impose the gauge-fixing condition $\Theta_x = 0$ of Eq. (28). $H_{\mathrm{RPA}}(Q)$ can now be separated into an intrinsic and rotational part:

$$H_{\mathrm{RPA}}(Q) = \sum_{\nu>0}\hbar\Omega_\nu O_\nu^\dagger O_\nu + \frac{J_x^2}{2\mathcal{J}_x}. \tag{47}$$

Thus, the zero-frequency mode can be eliminated from the RPA equation and $C_{\mathrm{RPA}}(Q)$ can be written as

$$C_{\mathrm{RPA}}(Q) = C'_{\mathrm{RPA}}(Q)e^{-\frac{J_x^2}{2\mathcal{J}_x}\beta}, \tag{48}$$

where $C'_{\mathrm{RPA}}(Q)$ is the correlation factor in the absence of zero-frequency modes.

In a similar fashion, spurious modes should be eliminated from the pairing RPA corrections of Eq. (40). This is not done in the present work since (i) exact number projection is needed for this procedure and (ii) the corrections are thought to be small in our number-parity projection scheme.

B. Moment of inertia

To connect with the result of Thouless and Valatin [30], we introduce the function

$$G = i\mathcal{J}_x\Theta_x/\hbar = \sum_{k,l}[g_{kl}(u_k v_l a_k^\dagger a_{\bar{l}}^\dagger - v_k u_l a_{\bar{l}} a_k) - \tilde{g}_{kl}(u_k u_l a_k^\dagger a_l - v_k v_l a_{\bar{l}}^\dagger a_{\bar{k}}]. \tag{49}$$

Then the Thouless-Valatin equations become

$$\langle[H_{\mathrm{RPA}}, G]_{\mathrm{PB}}\rangle = \langle J_x\rangle, \tag{50}$$

$$\langle[J_x, G]_{\mathrm{PB}}\rangle = \mathcal{J}_x. \tag{51}$$

Inserting Eq. (49) in the Thouless-Valatin equations yields

$$\hbar(j_x)_{kl} = (E_k + E_l)g_{kl} - \chi\sum_{mn}[Q_{kl}g_{mn} - \tilde{Q}_{kl}\tilde{g}_{mn} + Q_{kl}g_{mn}^* - \tilde{Q}_{kl}\tilde{g}_{mn}^*]Q_{mn}, \tag{52}$$

$$\hbar(j_x)_{kl} = (E_k - E_l)\tilde{g}_{kl} - \chi\sum_{mn}[Q_{mn}g_{mn} - \tilde{Q}_{mn}\tilde{g}_{mn} + Q_{mn}g_{mn}^* - \tilde{Q}_{mn}\tilde{g}_{mn}^*]\tilde{Q}_{kl}, \tag{53}$$

and the moment of inertia

$$\mathcal{J}_x = \hbar\sum_{k,l}(j_x)_{kl}[g_{lk}(u_k v_l - v_k u_l)^2(1 - f_k - f_l) + \tilde{g}_{lk}(u_k u_l + v_k v_l)^2(f_k - f_l)], \tag{54}$$

where we used the relations

$$g_{lk} = -g_{\bar{k}\bar{l}}, \quad \tilde{g}_{lk} = -\tilde{g}_{\bar{k}\bar{l}}, \qquad u_k = u_{\bar{k}}, \quad v_k = -v_{\bar{k}}. \tag{55}$$

Neglecting the two-body potential matrix elements in Eqs. (52) and (53), we can approximate g_{lk} and $\tilde{g}_{lk}$ by

$$g_{kl} = \hbar\frac{(j_x)_{kl}}{(E_k + E_l)}, \quad \tilde{g}_{kl} = \hbar\frac{(j_x)_{kl}}{(E_k - E_l)}, \tag{56}$$

and the moment of inertia at finite temperature simplifies to

$$J_x = 2\hbar^2\sum_{k,l>0}\frac{(j_x)_{kl}^2}{(E_k + E_l)}(u_k v_l - v_k u_l)^2(1 - f_k - f_l) + 2\hbar^2\sum_{k,l>0}\frac{(j_x)_{kl}^2}{(E_k - E_l)}(u_k u_l + v_k v_l)^2(f_k - f_l). \tag{57}$$

[1] Note that the zero-frequency mode (Goldstone mode) in the mean field plus RPA may become nonzero (imaginary or complex) in the SPA+RPA.

In the $T \to 0$ limit, the moment of inertia becomes the well-known Belyaev formula [31]

$$J_x = 2\hbar^2 \sum_{k,l>0} \frac{(j_x)^2_{kl}}{(E_k + E_l)} (u_k v_l - v_k u_l)^2. \quad (58)$$

Inserting Eqs. (46)–(48) into the partition function (28) under consideration of the gauge-fixing conditions $\hbar I = J_x$ and $\Theta_x = 0$, we obtain the partition function for an axially symmetric nucleus,

$$Z_{s,I} = \frac{2\beta}{G} \left(\frac{\kappa\beta}{2\pi}\right)^{5/2} \int_0^\infty d\Delta\Delta \int_0^\infty d\beta_2 \beta_2^4 Z_s(\Delta, \beta_2) \times 4\pi I^2 \exp\left(-\frac{\hbar^2 I^2}{2\mathcal{J}_x}\beta\right), \quad (59)$$

where

$$Z_s(\Delta, \beta_2) = \exp\left[-\left(\frac{\Delta^2}{G} + \frac{1}{2}\kappa\beta_2^2\right)\beta\right] \times Z_s^{\rm qp} C'_{\rm RPA}(Q) C_{\rm RPA}(\Delta), \quad (60)$$

and $Z_s^{\rm qp}$ is the quasiparticle partition function with the number-parity projection,

$$Z_s^{\rm qp} = \tfrac{1}{2}\prod_k e^{-\gamma_k\beta}(1 + e^{-E_k\beta})^2\left[1 + s\prod_{k'}\tanh^2(E_{k'}\beta)\right], \quad (61)$$

with $\gamma_k = \varepsilon_k - \mu - E_k$.

C. Level density

The level density for a system with a fixed number of particles can be evaluated by an inverse Laplace transformation of the partition function $Z_{s,I}$:

$$\rho(E, I) = \frac{1}{2\pi i} \int_{\beta_0 - i\infty}^{\beta_0 + i\infty} d\beta e^{\beta E} Z_{s,I}(\beta). \quad (62)$$

In the saddle-point approximation, the level density is given by

$$\rho(E, I) \approx \frac{Z_{s,I} e^{\beta E}}{[2\pi\,\partial^2 \ln Z_{s,I}/\partial\beta^2]^{1/2}}. \quad (63)$$

We will now apply the saddle-point approximation[2] to the two integrals in the partition function $Z_{s,I}$ of Eq. (59). However, Eq. (59) still contains the $2I + 1$ degeneracy connected to the magnetic quantum number. To determine the level density (as opposed to the state density), we make the transformation $I \to I + 1/2$ and $I^2 \to I(I+1)$ in Eq. (59) from a classical to a quantal angular momentum and divide by $2I + 1$.[3] Entering this modified partition function (59) into the saddle-point approximation for the level density (63), we finally obtain

$$\rho(E, I) \approx \rho(E) \frac{\hbar^2\beta}{2\mathcal{J}_x}(2I + 1) \exp\left(-\frac{\hbar^2 I(I+1)}{2\mathcal{J}_x}\beta\right), \quad (64)$$

where the total level density is given by

$$\rho(E) = \frac{\bar{Z}_s e^{\beta E}}{[2\pi\,\partial^2 \ln \bar{Z}_s/\partial\beta^2]^{1/2}}, \quad (65)$$

with

$$\bar{Z}_s = \frac{2\beta}{G}\left(\frac{\kappa\beta}{2\pi}\right)^{5/2} \frac{\Delta\beta_2^4 Z_s(\Delta, \beta_2)}{\sqrt{\det(B)}}, \quad (66)$$

and B is the fluctuation matrix

$$B_{ij} = \frac{\partial^2 \ln\left(\Delta\beta_2^4 Z_s(\Delta, \beta_2)\right)}{\partial y_i \partial y_j}, \quad (67)$$

with $y = (\Delta, \beta_2)$.

The level density (64) is the relevant spin-dependent microscopic level density for reaction cross-section calculations in the presence of correlations. By entering the partition function (60) in Eqs. (66) and (67), we can calculate this level density as a function of excitation energy, where the thermal energy can be calculated from $E = -\partial \ln \bar{Z}_s/\partial\beta$. Comparing this level density with the spin-cutoff model given in Eq. (1), we can relate the spin-cutoff parameter σ^2 to the moment of inertia $\mathcal{J}_x$ by

$$\sigma^2 = \frac{\mathcal{J}_x T}{\hbar^2}. \quad (68)$$

In the next section, we shall perform numerical calculations and show that there is a notable difference between the shape of the level density and the state density, which contains the factor $2I + 1$ because of the m degeneracy.

V. NUMERICAL CALCULATIONS

We consider ^{56}Fe [5,32] as an illustrative example. Recently, the level density in ^{56}Fe has been measured nearly up to the neutron binding energy [33–35]. In our calculation, we use the single-particle energies ε_k given by an axially deformed Woods-Saxon potential with spin-orbit interaction [36]. The Woods-Saxon parameters are chosen such as to approximately reproduce the experimental single-particle energies extracted from the energy levels of the odd nucleus ^{41}Ca (^{40}Ca core plus one neutron). Fifteen doubly-degenerate single-particle levels for neutrons and protons outside the ^{40}Ca core are considered; continuum levels are neglected since their contributions are small [8]. We adjust the pairing-force strengths at $G_n = 25/A$ MeV and $G_p = 29/A$ MeV for neutrons and protons, respectively, and the QQ-force strength at $\chi = 240/A^{5/3}b^4$. As mentioned, the SPA+RPA breaks down at low temperature. However, it has recently been shown that in the monopole pairing case the SPA+RPA with number-parity projection reproduces well exact results even for low temperatures [15]. Therefore, number-parity projection is essential to describe the thermal properties at low temperature. Calculations are

[2]The maximum in the saddle-point approximation leads to an effective mean-field equation; hence, a sharp phase transition as predicted by the ordinary mean-field equation is avoided.

[3]To keep in contact with experiment, we will consider this pseudo partition function for the remainder of this work and determine consistently all quantities from there.

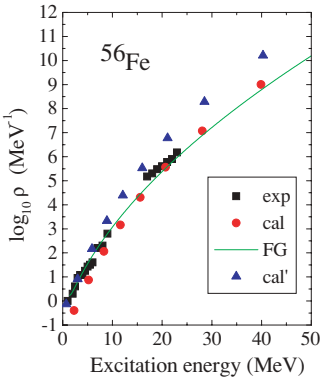

FIG. 1. (Color online) Experimental (squares) and calculated level densities $\rho(E)$ as a function of excitation energy in ^{56}Fe. Full circles and triangles denote the level and state density, respectively, from SPA+RPA calculations. The solid line is a back-shifted Fermi-gas model.

shown in Fig. 1. The level density calculated with the SPA+RPA reproduces fairly well the slope and magnitude of the experimental data. However, besides the expected difference in magnitude, the calculated state density, which contains the m degeneracy, also shows a different slope on the logarithmic plot. The calculations thus indicate an increase of $\sigma \propto \langle I \rangle$ with excitation energy; see also Eq. (68).

Figure 1 also shows a back-shifted Fermi-gas model [2–6] according to

$$\rho_{\mathrm{BSFG}}(E) = \frac{\exp[2\sqrt{aU}]}{12\sqrt{2}a^{1/4}U^{5/4}\sigma}, \tag{69}$$

where the back-shifted energy is $U = E - E_1$ and the spin-cutoff parameter σ is $\sigma^2 = 0.0888A^{2/3}\sqrt{aU}$ [3]. The level-density parameter a and the parameter E_1 are given by $a = A/10 = 5.6\ \mathrm{MeV}^{-1}$ and $E_1 = 1.0$ MeV, respectively. The level density from SPA+RPA calculations is close to that of the back-shifted Fermi-gas model for a wide range of excitation energies.

Figure 2 shows the calculated heat capacity for ^{56}Fe. The SPA+RPA deviates from the SPA result for temperatures

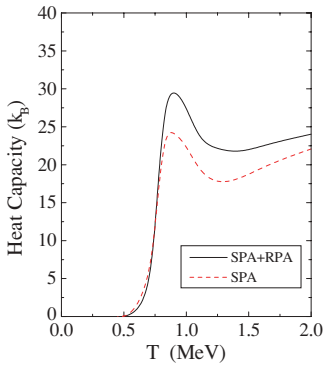

FIG. 2. (Color online) Heat capacities as a function of temperature T in ^{56}Fe. The solid and dotted curves denote the calculated heat capacities in the SPA+RPA and SPA, respectively. Both curves exhibit clear $\mathcal{S}$ shapes.

above $T = 0.9$ MeV; quantal fluctuations become important in this region. This behavior is consistent with the one found in Ref. [37]. Both of our results exhibit a characteristic $\mathcal{S}$ shape around $T_c \sim 0.9$ MeV. This critical temperature is higher than the SMMC result[4] (∼0.7 MeV) [38] but it is still smaller than the experimental one (∼1.3 MeV) [34]. Level densities in several nuclei have recently been measured [39,40] and the suppression of pairing correlations was studied in detail [41,42]. $\mathcal{S}$-shaped heat capacities with $T_c \sim 0.5$ MeV were also observed in ^{162}Dy, ^{166}Er, and ^{172}Yb [43,44]; they were interpreted as a signature of the breaking of nucleon Cooper pairs. We suggested that the suppression of pairing correlations at finite temperatures should also appear in the thermal odd-even mass differences [41,42]. In general, the $\mathcal{S}$ shape of the heat capacity has been attributed to the reduction of the pairing energy, which can be calculated from $G_\tau\langle P^\dagger P\rangle = G_\tau T\partial \ln \bar{Z}_s/\partial G_\tau$ [38]. In fact, this pairing reduction can be seen in thermal odd-even mass differences extracted from the experimental level densities [41,42,45]. However, it has been argued that the $\mathcal{S}$ shape might be accounted for as an effect of particle-number conservation on the quasiparticle excitations [46]. Nonetheless, even without exact particle-number projection, the SPA gives an $\mathcal{S}$-shaped heat capacity. In this sense, we emphasize that this $\mathcal{S}$ shape cannot be explained solely as an effect of the particle-number projection.

Figure 3(a) shows the effective pairing gap defined by

$$\Delta^\tau_{\mathrm{eff}} = G_\tau \left[\frac{1}{\beta}\frac{\partial \ln \bar{Z}_s}{\partial G_\tau}\right]^{1/2}. \tag{70}$$

Both Δ^n_{eff} and Δ^p_{eff} decrease in a similar fashion around $T = 0.9$ MeV, although the proton pairing is a little bit stronger than the neutron pairing. We can now identify the inflection point of the Δ_{eff} curves as the critical temperature of a pairing phase transition. To determine the position of the inflection point precisely, we differentiate the Δ_{eff} curves with respect to the temperature [see Fig. 3(b)]. From the peaks of these derivatives we read off a critical temperature around $T = 0.9$ MeV. Hence, the suppression of Δ_{eff} is well correlated with the $\mathcal{S}$ shape of the heat capacity. As pointed out in our previous paper [41], the critical temperature T_c is proportional to the pairing gap Δ. This is expressed by the relation $T_c \approx 0.57\Delta$ from Bardeen-Cooper-Schrieffer (BCS) theory. The critical temperature $T_c \approx 1.0$ MeV estimated from this relation is close to the position ∼0.9 MeV of the peaks in Fig. 3(b).

We will now apply a similar analysis to the moment of inertia. Figure 4(a) shows the moment of inertia as a function of temperature T. For comparison we also show the rigid-body value $\mathcal{J}_{\mathrm{rigid}} = 0.0137A^{5/3}\ \mathrm{MeV}^{-1}$ denoted by a dashed line. The calculated moment of inertia is smaller than the rigid-body value at low temperature. This strong suppression is a well-known effect from the presence of pairing correlations in low-lying, superfluid-like BCS states. For high temperatures,

[4]We would like to emphasize that, in contrast to the present calculation and the experiment, the SMMC result is obtained from a partition function that includes the m degeneracy.

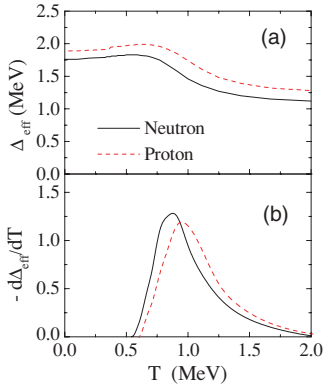

FIG. 3. (Color online) Effective pairing gaps (a) and their derivatives (b) as a function of temperature for ^{56}Fe. The solid and dotted curves are for neutrons and protons, respectively.

however, the calculation approaches the rigid-body value because the nucleon Cooper pairs break with increasing temperature. Again, we can define the critical temperature of the pairing phase transition as the inflection point, which is determined precisely by differentiation. Differentiation of the $\mathcal{J}_x$ curves reveals peaks around the critical temperature of $T = 0.9$ MeV [see Fig. 4(b)]. Hence, the increase of $\mathcal{J}_x$ is well correlated with both the $\mathcal{S}$ shape of the heat capacity in Fig. 2 and the suppression of the effective pairing gaps in Fig. 3.

To investigate more closely the relation between the effective gaps and the moment of inertia, we examine the correlation of the average effective pairing gap $\Delta_{\rm eff} = (\Delta^n_{\rm eff} + \Delta^p_{\rm eff})/2$ with the moment of inertia (see Fig. 5). Above $\mathcal{J}_x \approx 5.0\ \hbar^2$/MeV, which corresponds to $T \approx 0.7$ MeV, this correlation is close to a straight line, whereas deviations from the line become apparent below this temperature. The observation of such a correlation across the critical temperature of $T \approx 0.9$ MeV means that the increase of the moment of inertia can be attributed to the suppression of the pairing correlation. This

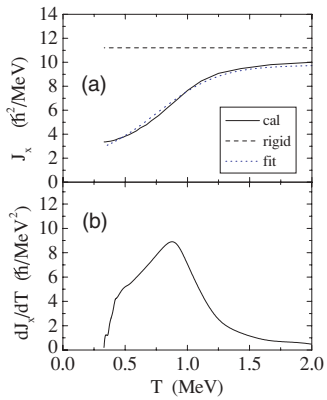

FIG. 4. (Color online) Moment of inertia (a) and the derivative (b) as a function of temperature for ^{56}Fe. The dashed line shows the rigid-body moment of inertia, the solid curve is the result of the SPA+RPA calculation, and the dotted curve is a fit to the calculation according to Eq. (73).

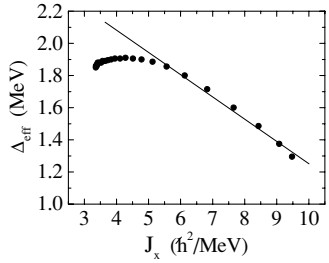

FIG. 5. Correlation of the average effective pairing gap with the moment of inertia. The straight line is to guide the eye.

conclusion has already been obtained by Alhassid *et al*. [8,9]. Thus the increase of the moment of inertia can be considered as another signature of the pairing phase transition together with the $\mathcal{S}$-shaped heat capacity [43,44] and the suppression of odd-even mass differences [41,42,45].

In the next step, we investigate the effect of the temperature-dependent moment of inertia on the spin distribution of nuclear levels for the ^{56}Fe case. For this purpose, we plot for the temperatures $T = 0.5$, 0.67, 1.0, and 2.0 MeV the spin distribution $\rho(E, I)/\rho(E)$ from Eq. (64) in Fig. 6. Moreover, we plot as a function of temperature the first μ_1 and second μ_2 moments of this spin distribution, where

$$\mu_1 = \frac{\sum_I f_I I}{\sum_I I}, \tag{71}$$

$$\mu_2 = \frac{\sum_I f_I (I - \mu_1)^2}{\sum_I I}, \tag{72}$$

and $f_I = \rho(E, I)/\rho(E)$ in Fig. 7, and finally, we plot again as a function of temperature the relative components of the spin distribution for the spins $I = 0$, 2, 4, and $6\hbar$. Comparing the SPA+RPA results to the spin-cutoff model based on a rigid-body moment of inertia, we observe from Figs. 6, 7, and 8 that good agreement between the two is

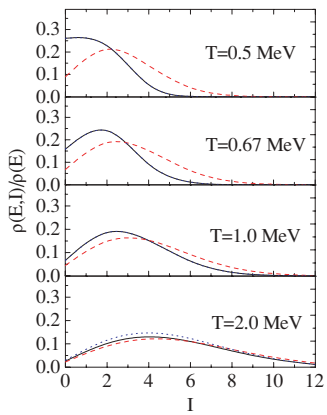

FIG. 6. (Color online) Spin distribution of level density at different temperatures T for ^{56}Fe. The SPA+RPA results (solid curves) are compared to the spin-cutoff model using the rigid-body moment of inertia (dashed curves) and the results from the fit to the moment of inertia according to Eq. (73) (dotted curves). The fit and the SPA+RPA calculations are almost indistinguishable.

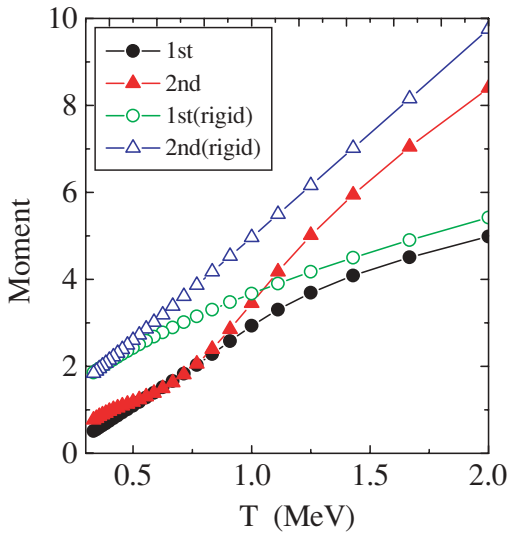

FIG. 7. (Color online) First (circles) and second (triangles) moments of the spin distribution as a function of temperature for ^{56}Fe. Results from the SPA+RPA calculation (full symbols) are compared to a model using the rigid-body moment of inertia (open symbols).

achieved at high temperatures ($T \gtrsim 2$ MeV). Deviations are, however, significant for lower temperatures. In particular, the $I = 0$ component is much larger than all other I components in the SPA+RPA calculation, whereas for the rigid-body spin-cutoff model, the largest component at low temperature is $I = 2$ but the $I = 0$ component is quite small. Around $T \sim 0.5$ MeV in the SPA+RPA calculation, the $I =$ 0 component quickly decreases with increasing temperature whereas the $I = 2$ component increases drastically up to $T = 0.7$ MeV where it becomes dominant, in agreement with the rigid-body spin-cutoff model. The $I = 4$ and 6 components also exhibit small magnitudes at low temperature and increase with increasing temperature.

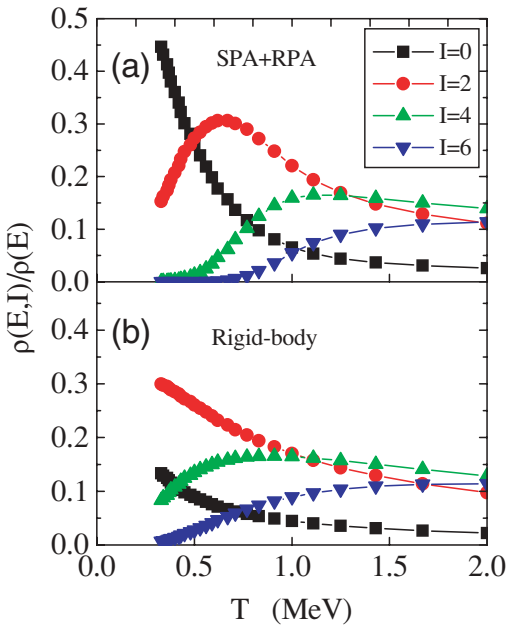

FIG. 8. (Color online) Spin components of level density as a function of temperature T for ^{56}Fe. The relative components for spins $J = 0$, 2, 4, and 6 are from SPA+RPA calculations (upper panel) and from a spin-cutoff model using the rigid-body moment of inertia (lower panel).

To conclude the discussion, we would like to make two remarks. First, the spin distributions in Fig. 6 can be very well described by a phenomenological model for the moment of inertia

$$\tilde{\mathcal{J}}_x = \mathcal{J}_{\text{rigid}} - \frac{c_1}{1 + \exp(c_2 T^2)} - c_3, \tag{73}$$

with the parameters $c_1 = 15.0\hbar^2/\text{MeV}$, $c_2 = 1.8\ \text{MeV}^{-2}$, and $c_3 = 1.5\hbar^2/\text{MeV}$. This model of the moment of inertia includes the effect of the quenching of pairing correlations. The three parameters of the model essentially determine the moment of inertia at zero temperature (in the presence of pairing correlations), the moment of inertia at very high temperature (in the absence of pairing correlations), and the critical temperature itself. Hence, the three parameters might be connected to collective $E2$ transition rates within rotational bands at low and high spin, respectively, and to odd-even mass differences via $T_c \approx 0.57\Delta$. This would be interesting to investigate since a simple phenomenological model of the moment of inertia based on experimental observables would be valuable for many applications of the nuclear level density such as Hauser-Feshbach-type cross-section calculations. Second, we note the presence of an $\mathcal{S}$ shape in the second moment of the spin distribution (see Fig. 7). This is in analogy to the $\mathcal{S}$ shape of the heat capacity (see Fig. 2), which in itself is proportional to the second moment of the excitation-energy distribution for a given T. We would therefore propose this $\mathcal{S}$ shape of the second moment as another signature of the pairing phase transition, and it would be interesting to look for experimental evidence for it.

VI. CONCLUSION

We have presented a treatment of nuclear rotation by the SPA+RPA method including thermal and quantal fluctuations. By using the collective coordinate method and applying a Marshalek-Weneser treatment, the RPA partition function is separated into two parts: an intrinsic RPA and a rotational part. We then can derive the spin-dependent level density $\rho(E, I)$ in the saddle-point approximation without the assumption of individual random spin vectors. The spin-cutoff parameter σ can be identified with the moment of inertia $\mathcal{J}_x$ of the generalized Belyaev formula. As an illustrative example, we have applied this method to ^{56}Fe and investigated the thermal properties, including the moment of inertia, with consideration of thermal and quantal fluctuations. We obtained the same conclusion as Alhassid *et al.* [8,9], namely that the increase of the moment of inertia with increasing temperature is attributed to the suppression of pairing correlations. The increase of the moment of inertia can therefore be considered as one of the signatures of the pairing phase transition in parallel with the $\mathcal{S}$ shape of the heat capacity and the suppression of

odd-even mass differences. The spin distribution of the level density shows that the $I = 0$ component is dominant at low temperatures owing to the presence of pairing correlation; this component decreases with increasing temperature. At high temperatures, the level density is governed by $I \neq 0$ components. In this work, we assumed an axially symmetric nucleus with $K = 0$ although our formulation can be easily extended to nonzero K quantum numbers. However, the K quantum number is thought to disappear because of K mixing at some excitation energy above the yrast line. For this mixing, another degree of freedom, namely γ deformation, is important. It would be very interesting to investigate this issue in the future.

ACKNOWLEDGMENTS

One of the authors (K.K.) would like to thank Dr. M. Hasegawa for fruitful and inspiring discussions. Financial support from the National Science Foundation under Grant No. PHY-06-06007 is gratefully acknowledged.

[1] T. Rauscher, F.-K. Thielemann, and K.-L. Kratz, Phys. Rev. C **56**, 1613 (1997).
[2] H. A. Bethe, Phys. Rev. **50**, 332 (1936).
[3] A. Gilbert and A. G. W. Cameron, Can. J. Phys. **43**, 1446 (1965).
[4] S. M. Grimes, J. D. Anderson, J. W. McClure, B. A. Pohl, and C. Wong, Phys. Rev. C **10**, 2373 (1974).
[5] C. C. Lu, L. C. Vaz, and J. R. Huizenga, Nucl. Phys. **A190**, 229 (1972).
[6] T. von Egidy, H. H. Schmidt, and A. N. Behkami, Nucl. Phys. **A481**, 189 (1988); T. von Egidy and D. Bucurescu, Phys. Rev. C **72**, 044311 (2005); **73**, 049901(E) (2006).
[7] T. Ericson, Adv. Phys. **9**, 425 (1960).
[8] Y. Alhassid, G. F. Bertsch, L. Fang, and S. Liu, Phys. Rev. C **72**, 064326 (2005).
[9] Y. Alhassid, S. Liu, and H. Nakada, nucl-th/0607062.
[10] Y. Alhassid and J. Zingman, Phys. Rev. C **30**, 684 (1984); Y. Alhassid and B. W. Bush, Nucl. Phys. **A549**, 43 (1992).
[11] P. Arve, G. Bertsch, B. Lauritzen, and G. Puddu, Ann. Phys. (NY) **183**, 309 (1988); B. Lauritzen, P. Arve, and G. F. Bertsch, Phys. Rev. Lett. **61**, 2835 (1988).
[12] R. Rossignoli, A. Ansari, and P. Ring, Phys. Rev. Lett. **70**, 1061 (1993); R. Rossignoli and P. Ring, Ann. Phys. (NY) **235**, 350 (1994).
[13] G. Puddu, P. F. Bortignon, and R. A. Broglia, Ann. Phys. (NY) **206**, 409 (1991); Phys. Rev. C **42**, R1830 (1990).
[14] B. Lauritzen, G. Puddu, P. F. Bortignon, and R. A. Broglia, Phys. Lett. **B246**, 329 (1990); B. Lauritzen, A. Anselmino, P. F. Bortignon, and R. A. Broglia, Ann. Phys. (NY) **223**, 216 (1993).
[15] R. Rossignoli, N. Canosa, and P. Ring, Phys. Rev. Lett. **80**, 1853 (1998); R. Rossignoli and N. Canosa, Phys. Lett. **B394**, 242 (1997).
[16] H. Attias and Y. Alhassid, Nucl. Phys. **A625**, 565 (1997).
[17] J.-L. Gervais and B. Sakita, Phys. Rev. D **11**, 2943 (1975); J. L. Gervais and A. Neveu, Phys. Rep. **23**, 237 (1976).
[18] J. L. Gervais, A. Jevicki, and B. Sakita, Phys. Rep. **23**, 281 (1976).
[19] V. Alessandrini, D. R. Bès, and B. Machet, Nucl. Phys. **B142**, 489 (1978).
[20] D. R. Bès, O. Civitarese, and H. M. Sofía, Nucl. Phys. **A370**, 99 (1981).
[21] L. S. Kisslinger and R. A. Sorensen, Rev. Mod. Phys. **35**, 853 (1963).
[22] D. R. Bes and R. A. Sorensen, Adv. Nucl. Phys. **2**, 129 (1969).
[23] G. Puddu, Phys. Rev. C **47**, 1067 (1993).
[24] J. Hubbard, Phys. Rev. Lett. **3**, 77 (1959); R. L. Stratonovich, Dokl. Akad. Nauk SSSR **115**, 1097 (1957).
[25] G. H. Lang, C. W. Johnson, S. E. Koonin, and W. E. Ormand, Phys. Rev. C **48**, 1518 (1993); S. E. Koonin, D. J. Dean, and K. Langanke, Phys. Rep. **278**, 1 (1997).
[26] C. Bloch and A. Messiah, Nucl. Phys. **39**, 95 (1962).
[27] K. Tanabe and N. D. Dang, Phys. Rev. C **62**, 024310 (2000).
[28] O. Civitarese, J. G. Hirsch, F. Montani, and M. Reboiro, Phys. Rev. C **62**, 054318 (2000).
[29] E. R. Marshalek and J. Weneser, Ann. Phys. (NY) **53**, 569 (1969).
[30] D. J. Thouless and J. G. Valatin, Nucl. Phys. **31**, 211 (1962).
[31] S. T. Beliaev, Nucl. Phys. **24**, 322 (1961).
[32] J. R. Huizenga, H. K. Vonach, A. A. Katsanos, A. J. Gorski, and C. J. Stephan, Phys. Rev. **182**, 1149 (1969).
[33] A. Schiller *et al*., Phys. Rev. C **68**, 054326 (2003).
[34] E. Tavukcu *et al*., AIP Conf. Proc. **656**, 136 (2003).
[35] A. V. Voinov *et al*., Phys. Rev. C **74**, 014314 (2006).
[36] S. Cwiok, J. Dudek, W. Nazarewicz, J. Skalski, and T. Werner, Comput. Phys. Commun. **46**, 379 (1987).
[37] N. Canosa, R. Rossignoli, and P. Ring, Phys. Rev. C **59**, 185 (1999).
[38] S. Liu and Y. Alhassid, Phys. Rev. Lett. **87**, 022501 (2001).
[39] V. A. Bondarenko, J. Honzatko, V. A. Khitrov, L. Chol, Yu. E. Loginov, S. Eh. Malyutenkova, A. M. Sukhovoj, and I. Tomandl, in *Proceedings of the XII International Seminar on Interaction of Neutrons with Nuclei, Dubna, Russia, 2004*, p. 38; nucl-ex/040630.
[40] R. Chankova *et al*., Phys. Rev. C **73**, 034311 (2006).
[41] K. Kaneko and M. Hasegawa, Nucl. Phys. **A740**, 95 (2004).
[42] K. Kaneko and M. Hasegawa, Phys. Rev. C **72**, 024307 (2005).
[43] A. Schiller, A. Bjerve, M. Guttormsen, M. Hjorth-Jensen, F. Ingebretsen, E. Melby, S. Messelt, J. Rekstad, S. Siem, and S. W. Ødegård, Phys. Rev. C **63**, 021306(R) (2001).
[44] E. Melby, L. Bergholt, M. Guttormsen, M. Hjorth-Jensen, F. Ingebretsen, S. Messelt, J. Rekstad, A. Schiller, S. Siem, and S. W. Ødegård, Phys. Rev. Lett. **83**, 3150 (1999).
[45] K. Kaneko *et al*., Phys. Rev. C **74**, 024325 (2006).
[46] K. Esashika, H. Nakada, and K. Tanabe, Phys. Rev. C **72**, 044303 (2005).